Thermoelectric transport properties of silicon: Toward an *ab initio* approach

Zhao Wang,[1,*] Shidong Wang,[2] Sergey Obukhov,[3] Nathalie Vast,[4] Jelena Sjakste,[4] Valery Tyuterev,[3] and Natalio Mingo[1]

[1]*LITEN, CEA-Grenoble, 17 rue des Martyrs, 38054 Grenoble Cedex 9, France*

[2]*Department of Mechanical Engineering and Materials Science, Duke University, Durham, NC, 27708*

[3]*Tomsk State Pedagogical University, 634061 Kievskaya 60, Tomsk, Russia*

[4]*Ecole Polytechnique, Laboratoire des Solides Irradiés, CEA-DSM-IRAMIS, CNRS UMR 7642, 91120 Palaiseau, France*

(Received 23 November 2010; revised manuscript received 18 March 2011; published 23 May 2011)

We have combined the Boltzmann transport equation with an *ab initio* approach to compute the thermoelectric coefficients of semiconductors. Electron-phonon, ionized impurity, and electron-plasmon scattering mechanisms have been taken into account. The electronic band structure and average intervalley deformation potentials for the electron-phonon coupling were obtained from the density functional theory. The linearized Boltzmann equation has then been solved numerically beyond the relaxation-time approximation. Our approach has been applied to crystalline silicon. We present results for the mobility, Seebeck coefficient, and electronic contribution to thermal conductivity as functions of the carrier concentration and temperature. The calculated coefficients are in good quantitative agreement with experimental results.

DOI: 10.1103/PhysRevB.83.205208 PACS number(s): 84.60.Rb, 72.20.Pa

I. INTRODUCTION

Interest in thermoelectric materials has been rapidly growing in recent years. This is due in part to the new expectation of materials with a higher dimensionless figure of merit ZT brought about by the nanotechnology revolution.[1–4] From the theoretical point of view, it is important to be able to predict various thermoelectric properties without resorting to adjustable parameters. However, despite great advances in predicting the electronic structure of materials, calculation of thermoelectric transport properties from-first-principles still presents a challenge, even in the case of simple bulk materials.

In some relevant works, attempts have been made to use a from-first-principles description of the band structure, combined with the relaxation-time approximation (RTA) of the scattering mechanisms.[5–14] However, these approaches can still be considered as semiempirical, since the scattering rates depend on adjustable parameters, and moreover rely on approximations for their energy dependence. A recent calculation of the mobility of SiGe alloys has been presented in Ref. 15, where the scattering rates have also been computed from-first-principles in the RTA. Regarding silicon, its mobility has been explored employing a parameter-free approach[16] within the RTA,[17,18] and its lattice thermal conductivity has been computed *ab initio*, together with that of germanium and diamond.[19,20]

Thus previous *ab initio* works largely relied on the RTA, and in most cases, the *ab initio* aspect was limited to the calculation of electronic band structures. Our goal is to go beyond this stage by computing *ab initio* scattering rates, and solving the Boltzmann transport equation (BTE) beyond the RTA. In the present study we are focusing on the thermoelectric properties of crystalline silicon, despite the fact that it is not a good candidate for practical thermoelectric applications. However, its electronic properties have been intensively investigated in the scientific literature, with a large amount of theoretical studies devoted to the calculation of the mobility of silicon using adjustable parameters.[21–23] Si constitutes an ideal system to test the ability of *ab initio* methods to predict transport coefficients.

This paper is organized as follows. The general theory for the Boltzmann equation is presented in Sec. II. The *ab initio* method used to compute the band structure and the average deformation potentials for the intervalley electron-phonon scattering is described in Sec. III. Results are discussed in Sec. IV, and conclusions are drawn in Sec. V.

II. BOLTZMANN TRANSPORT EQUATION

The electron occupation distribution function f has been obtained by solving the BTE[24,26] for steady states in the presence of a uniform and static external electric field $\boldsymbol{E}$ and a temperature gradient ∇T,[25]

$$-\frac{\partial f}{\partial \varepsilon}\boldsymbol{v}\cdot\left(e\boldsymbol{E}+\nabla T\frac{\varepsilon-\varphi}{T}\right)=\frac{-V}{8\pi^3}\int[f(\boldsymbol{k})(1-f(\boldsymbol{k}'))\times S(\boldsymbol{k},\boldsymbol{k}')-f(\boldsymbol{k}')(1-f(\boldsymbol{k}))S(\boldsymbol{k}',\boldsymbol{k})]d\boldsymbol{k}', \quad (1)$$

where ε is the band energy associated with a point $\boldsymbol{k}$ in the semiclassical phase space, φ is the chemical potential, $\boldsymbol{v}$ is the electron velocity, V is the unit cell volume, and $S(\boldsymbol{k},\boldsymbol{k}')$ is the probability of a transition from $\boldsymbol{k}$ to $\boldsymbol{k}'$ per unit of time.

The linear approximation[26] consists of assuming that f can be written as a linear function of the applied external fields. At low field,

$$f(\boldsymbol{k})=f_0(\boldsymbol{k})+e\boldsymbol{E}\cdot\boldsymbol{v}(\boldsymbol{k})g(\boldsymbol{k})+\frac{\nabla T}{T}\cdot\boldsymbol{v}(\boldsymbol{k})g^*(\boldsymbol{k}), \quad (2)$$

where f_0 is the equilibrium Fermi–Dirac distribution and $g(\boldsymbol{k})$ and $g^*(\boldsymbol{k})$ are the first order corrections to f_0 due to the external electric field and temperature gradient. The approximation of nondegenerate statistics is not used in this work. The combination of Eq. (1) and Eq. (2) yields two linear matrix equations:

$$\boldsymbol{\xi}=(\boldsymbol{S}^{\text{out}}-\boldsymbol{S}^{\text{in}})\boldsymbol{g},$$
$$\boldsymbol{\xi}^*=(\boldsymbol{S}^{\text{out}}-\boldsymbol{S}^{\text{in}})\boldsymbol{g}^*, \quad (3)$$

where $\xi=(8\pi^3 v/V)(\partial f_0/\partial\varepsilon)$ and $\xi^*=(\varepsilon-\varphi)\xi$, $\boldsymbol{\xi}$ and $\boldsymbol{g}$ are n-component vectors. $\boldsymbol{S}^{\text{out}}$ and $\boldsymbol{S}^{\text{in}}$ are $n\times n$ matrices, where n is the total number of $\boldsymbol{k}$ points. $\boldsymbol{S}^{\text{out}}$ is diagonal

with $S_{i,i}^{\text{out}} = \sum_{j=1}^{n}[S_{j,i} f_0^j + S_{i,j}(1 - f_0^j)]$. $\boldsymbol{S}^{\text{in}}$ reads $S_{i,j}^{\text{in}} = S_{i,j} f_0^i + S_{j,i}(1 - f_0^i)$, with $S_{j,i}$ referring to $S(\boldsymbol{k}_j, \boldsymbol{k}_i)$. An energy range of 0.13 eV near the bottom of the conduction band has been discretized with 40 energy values. For each value of the energy ε, Eqs. (3) have been solved for a set of $\boldsymbol{k}$ vectors on the surface of constant energy. In our calculation, discretization of the Brillouin zone (BZ) is performed using the Gilat–Raubenheimer procedure (see next section).

The matrix elements of $\boldsymbol{S}$ have been computed by considering different scattering mechanisms, including electronic interactions with intravalley and intervalley phonons, ionized impurities and plasmons,

$$S = S^{\text{intra}} + S^{\text{inter}} + S^{\text{imp}} + S^{plsm}, \tag{4}$$

where S^{intra} represents the electronic scattering by a phonon of vanishing wave vector $\boldsymbol{q} = \boldsymbol{0}$, for which, in the scattering process, the initial and final electronic states are located in the same valley. The term S^{inter} represents the electronic scattering by a phonon of finite wave vector $\boldsymbol{q} \neq \boldsymbol{0}$, the intervalley scattering, in which the initial and final electronic states belong to two different valleys. In silicon, this mechanism involves a scattering from the valley Δ, located near the X point, to one of the five other equivalent Δ' valleys with $\boldsymbol{k}' = \boldsymbol{k} + \boldsymbol{q}$. The matrix S^{imp} represents the scattering probability of the electrons by the impurities. The first three scattering processes, S^{intra}, S^{inter} and S^{imp}, have been calculated using models described in Jacoboni and Reggiani.[21] The deformation potentials used to compute S^{inter} have been calculated *ab initio* as described in the next section. For electronic interactions with zone-center acoustic phonons S^{intra}, we have used the elastic approximation, assuming the phonon energy to be negligible. The intervalley scattering is an inelastic process, with scattering probability S^{inter}, which reads[21]

$$S_{i,j}^{\text{inter}} = \frac{\pi}{V \eta \omega_{ph}} D^2 N_{ph} \delta(\varepsilon_i - \varepsilon_j - \hbar\omega_{ph}). \tag{5}$$

Here, V is the unit cell volume, η is the crystal mass density, ω_{ph} and D are the effective phonon frequency and deformation potential, characterizing a particular intervalley scattering channel, N_{ph} is the phonon occupation number, and ε_i and ε_j are the energies of the initial and final electronic states. In our calculations, the following approximation has been made:

$$\begin{aligned} &f_0(\varepsilon_i)\delta(\varepsilon_i - \varepsilon_j \pm \hbar\omega_{ph}) \\ &\quad \approx \delta(\varepsilon_i - \varepsilon_j) f_0(\varepsilon_i \pm \hbar\omega_{ph}) \frac{\rho(\varepsilon_i \pm \hbar\omega_{ph})}{\rho(\varepsilon_i)}, \end{aligned} \tag{6}$$

where ρ is the density of states. Finally, S^{plsm} stands for the electron-plasmon interaction probability, and has been calculated using Fischetti's approach.[22]

Once the value of the distribution function f was determined, the electrical conductivity σ can be calculated as

$$\sigma = \frac{2e}{8\pi^3} \int g(\boldsymbol{k}) \frac{\boldsymbol{v} \cdot \boldsymbol{E}}{|\boldsymbol{E}|} d\boldsymbol{k}. \tag{7}$$

The electron mobility is given by

$$\mu = \frac{\sigma}{eN}, \tag{8}$$

where N is the carrier concentration.

The Seebeck coefficient (thermopower) Q has been calculated from the solution of g, using

$$\sigma Q = \frac{2e}{8\pi^3 T} \int (\varepsilon - \varphi) g \boldsymbol{v} \cdot \frac{\boldsymbol{E}}{|\boldsymbol{E}|} d\boldsymbol{k}. \tag{9}$$

Finally, the expression used to evaluate the electronic contribution to the thermal conductivity κ was

$$\kappa = -T\sigma Q^2 + \frac{2e}{8\pi^3} \int (\varepsilon - \varphi) g^* \boldsymbol{v} \cdot \frac{\boldsymbol{E}}{|\boldsymbol{E}|} d\boldsymbol{k}. \tag{10}$$

III. *AB INITIO* CALCULATIONS

The BTE is coupled with the band structure of silicon computed from-first-principles, and with the electron-phonon coupling constants obtained *ab initio* for the intervalley scattering.[27–31] The calculations have been performed respectively within the density functional theory[32,33] (DFT) and the density functional perturbation theory[34,35] (DFPT). The local density approximation (LDA) has been used for the exchange and correlation functional. We have used the pseudopotential and plane-wave approach to solve the Kohn–Sham equations. For silicon, the pseudopotential of Refs. 31,36 has been used, and the size of the plane-wave basis set has been limited with a cutoff energy of 45 Ry. Finally, a $4 \times 4 \times 4$ Monkhorst–Pack grid has been used to sample the BZ, yielding 10 non–equivalent $\boldsymbol{k}$ points in the irreducible BZ. We have obtained an equilibrium lattice parameter a of 5.40 Å for silicon, and the conduction band minimum Δ in the irreducible BZ was at $k_s = (0,0,k_0)\frac{2\pi}{a}$, with $k_0 = 0.84$ in our calculations[31] and $k_0 = 0.85$ in the literature.[37]

Each isosurface has been defined by a given energy value above the conduction band edge ε and has been determined from-first-principles. To obtain the $\boldsymbol{k}$ points forming the isosurface, we have first divided the irreducible BZ into a set of small parallelepipeds, $l_x = \mathbf{b}_x/N_x$, $l_y = \mathbf{b}_y/N_y$, $l_z = \mathbf{b}_z/N_z$, where b_α and N_α are the unit reciprocal lattice vectors and the number of segments in the direction α, respectively. In each elemental parallelepiped, a representative $\boldsymbol{k}$ point at the given value of ε has been obtained with Brent's method.[38] The weight of the selected $\boldsymbol{k}$ point has been computed as the area of the energy surface confined in the parallelepiped. This area has been calculated using the method proposed by Gilat and Raubenheimer.[39] The constant-energy surface in the parallelepiped has been approximated by a plane intersecting with the parallelepiped. The plane has been chosen according to the energy gradient at the representative $\boldsymbol{k}$ point. The details of the method can be found in Ref. 39. When the parallelepiped was small enough, the plane proved to be a very good approximation to the constant-energy surface.

In the BTE, the implementation of the electronic scattering by the short-wavelength phonons, S^{inter}, has been performed with average deformation potentials computed *ab initio* (Table I). Details about the f-TA (transverse acoustic) and g-LA (longitudinal acoustic) processes have been reported elsewhere.[31] The latter processes are forbidden by the symmetry selection rules to zeroth order, when the phonon wave-vector $\boldsymbol{q}$ is strictly equal to the vector connecting the bottoms of the two valleys Δ or Δ'. The scattering processes are, however, allowed for phonon vectors that connect points

TABLE I. Deformation potentials for the intervalley scattering: effective deformation potentials and phonon frequencies of Ref. 21 (columns 3 and 4) and *ab initio* average deformation potentials (column 4, the value of D has been averaged over states in the final valley for f processes, and over both initial and final valleys for g processes[40]) and phonon frequencies (last two columns). The average over states in the final valley only for g-processes yields values of the deformation potentials very similar, namely (in eV/Å): $D_T A = 0.60, D_L A = 1.20, D_T O = 1.19$ and $D_L O = 4.10$.

		Jacoboni and Reggiani[a]		This work		
	phonon label	D (eV/Å)	ω (K)	D (eV/Å)	(K)	ω (THz)
g processes	TA	0.5	140	0.61[b]	138	2.88
	LA	0.8	215	1.22[b]	226	4.72
	TO			1.26[b]	698	14.56
	LO	11.0	720	4.18[c]	720	15.01
f-processes	TA_1	0.3	220	0.18[b]	217	4.52
	TA_2			0.20[b]	263	5.48
	LA	2.0	550	1.12[c]	521	10.86
	LO			2.08[b]	569	11.86
	TO_1	2.0	685	2.40[b]	658	13.72
	TO_2			4.24[c]	669	13.95

[a]From Table VI of Ref. 21.
[b]First-order transition (see text).
[c]Zeroth order transition.

in the neighborhood of Δ or Δ' (first-order processes). The matrix elements for these first-order scattering processes have been computed on a grid with a step of $0.02\frac{2\pi}{a}$, and have been averaged by fixing the initial electronic states at the Δ point and by summing the matrix elements over final electronic states close to the Δ' point. The above-defined grid restricts the intervalley scattering to the processes involving energy values up to 100 meV above the conduction band edge. Average deformation potentials of 0.2 eV/Å for f-TA and 1.2 eV/ Å for g-LA processes have been obtained.[31] These values are close to the values of 0.3 eV/ Å and 0.8 eV/ Å used in Monte Carlo simulations (column 3 of Table I).[21]

In contrast with the averaged values for the f-TA and g-LA processes, however, our *ab initio* averaged values for the intervalley scattering by other phonons can be widely different from the set of deformation potentials of Ref. 21. This appears to be especially true for the scattering by the g-LO phonon (Table I) and illustrates the need for parameter free calculations. Moreover, our calculations provide additional values for the scattering involving g-TO or f-LO phonons, which have been neglected so far in the modeling based on empirical deformation potentials (Table I). Last, *ab initio* calculations enable us to discriminate between the deformation potentials of the transverse phonons, which have been considered as degenerate in previous works.[21] While this approximation is valid for the f-TA intervalley processes, because the *ab initio* values of f-TA_1 and f-TA_2 are very similar, some caution must be taken with the scattering involving f-TO_1 or f-TO_2 phonons, for which we have found substantially different values of the deformation potentials (Table I).

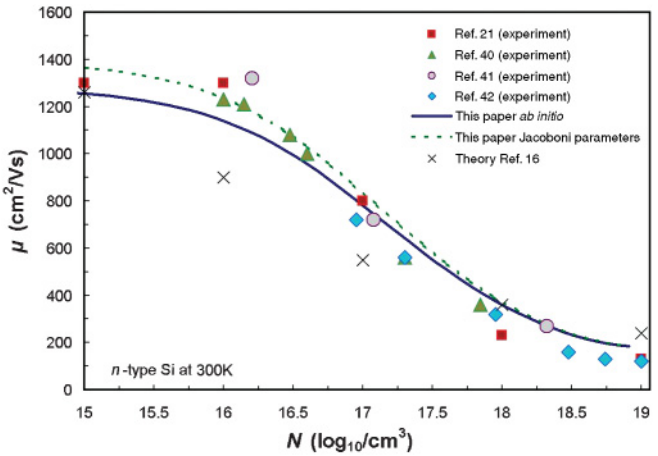

FIG. 1. (Color online) Electronic mobility μ versus the carrier concentration N for n-doped Si at $T = 300$ K. Solid and dashed lines are our results computed using deformation potentials for the intervalley scattering from our *ab initio* calculations and from Ref. 21, respectively. Crosses: theoretical results of Ref. 16. The symbols stand for experimental data. Squares, triangles, circles, and diamonds are results of Refs. 21, 40, 41 and 42 respectively.

IV. RESULTS AND DISCUSSION

To make a valid comparison with the experimental results, the effects of all of the scattering mechanisms described in Sec. II have been taken into account. In Fig. 1, the electronic mobility has been computed with both sets of intervalley deformation potentials presented in Table I, i.e., those computed *ab initio* (solid line) and those of Jacoboni and Reggiani, Ref. 21 (dashed line). The parameters for the other scattering processes were taken from Ref. 22. In both cases we have used the DFT band structure. The comparison between our calculated electronic mobility and the experimental one (symbols) shows an excellent agreement over the whole range of carrier concentrations.

The mobility calculated using the empirical deformation potential values from Ref. 22 is higher than that obtained from the DFT-calculated ones. In fact, the empirical deformation potentials of Jacoboni and Reggiani,[1] were adjusted to obtain the best fit to experimental data. We attribute the difference between the two curves to the increase in the number of scattering channels for the intervalley scattering computed *ab initio* (see Table I). In the high-concentration region ($N > 10^{18}\text{cm}^{-3}$), the electron-phonon interaction is negligible, and the two curves coincide.

Compared with the theoretical work of Ref. 16 (Fig. 1, crosses), which used from-first-principles calculations, our results give somewhat better agreement with the experimental data. We do not consider that reason comes from a difference in the treatment of the electron-phonon scattering, as the RTA approximation applied to Eq. (2) of Ref. 16 amounts to the calculation of the average deformation potentials, as we have done in Table I. Rather, several reasons can give rise to the observed differences. First, the solution of the BTE was performed in the RTA in Ref. 16, i.e., only the S^{out} matrix has been taken into account in Eq. (3). We have improved over the RTA approximation by taking into account $S^{\text{out}} - S^{\text{in}}$. Second, the elastic scattering by ionized impurities has been

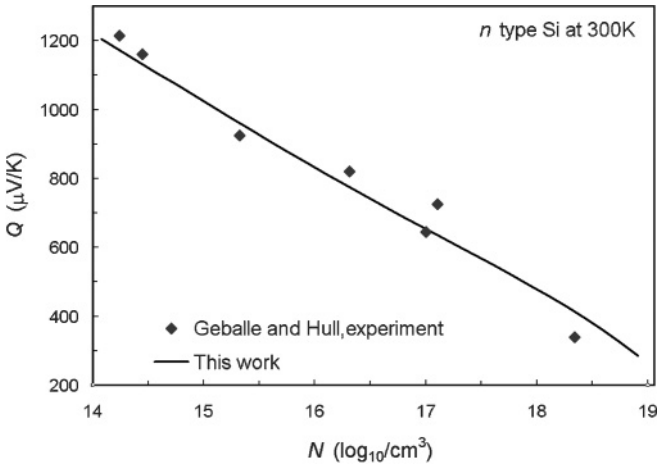

FIG. 2. Seebeck coefficient Q versus carrier concentration N for n-doped Si at $T = 300$ K. Solid line: this paper. Diamonds: experimental results from Ref. 43, where N has been calculated by us as $N_d - N_{ac}$, where N_d and N_{ac} are, respectively, the donor and acceptor concentrations.

computed *ab initio* in Ref. 16, whereas we still rely on the model of Jacoboni and Reggiani,[21] adjusted by the best fit to the experimental data. Last, in contrast to the work of Ref. 16, we have included electron-plasmon interaction as in Ref. 22, which becomes important in the high doping regime ($N > 10^{17}$ cm^{-3}).

Perfect agreement of our results with the existing experimental data[43] is shown in Fig. 2 for the Seebeck coefficient Q. No significant difference in Q has been found between the values calculated using the *ab initio* deformation potentials and those obtained with the empirical parameters of Ref. 21.

Thermal and electric transport properties of Si have been intensively studied in the past.[21,22] However, very few works gave thermoelectric coefficients over a wide range of doping concentrations and temperatures in a systematic way. To fill this gap, we have systematically computed electronic mobility μ, electrical conductivity σ, Seebeck coefficient Q, and thermal conductivity κ as a function of the temperature T for different doping concentrations, which correspond to different values of the chemical potential φ. In Fig. 3(a), significant increase of μ can be observed when the temperature decreases below 150 K, in agreement with the inverse power scaling law $\mu \propto 1/T^a$, where a is a positive number increasing with $|\varphi|$.[44] The electrical conductivity $\sigma = eN\mu$ increases with T, since more carriers are generated at higher temperatures for a given φ, despite the decrease of μ with temperature. It can be seen that, for a given T, σ has the highest value when the value of φ is close to the bottom of the lowest conduction band [panel (b)]. The value of Q, the thermal power, decreases when the temperature increases at a given chemical potential [panel (c)], as expected from Eq. (9). The thermal conductivity κ increases with the temperature at a given φ. This trend is, however, different from that observed for nanowires, where thermal transport is dominated by phonons.[46]

We have also studied the effect of doping on the thermoelectric properties at given temperatures. The value of the electronic mobility μ is almost constant in the low concentration region of $N < 10^{16}$ cm^{-3}, and then it rapidly

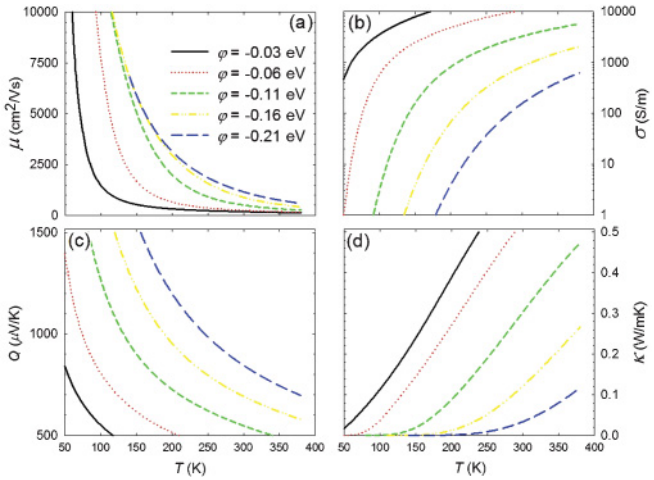

FIG. 3. (Color online) Thermoelectric properties of n-doped Si as a function of the temperature (T) for five values of the chemical potential φ. (a) electronic mobility; (b) electrical conductivity; (c): Seebeck coefficient (or thermal power); (d): electronic contribution to the thermal conductivity. For the calculation of φ the energy of the bottom of the conduction band has been set to zero.

decreases when N becomes larger than 10^{16} cm^{-3} [panel (a) of Fig. 4]. It can be seen that σ linearly increases with increasing N for weak doping, since μ is constant in this doping range [panel (b) of Fig. 4]. At higher carrier concentrations, the increase becomes less significant because of the decrease in the mobility. Furthermore, Q decreases almost linearly with increasing $\log(N)$ [panel (c) of Fig. 4]. The electronic contribution to the thermal conductivity κ also sensitively depends on the carrier density in the conduction band [panel (d) of Fig. 4]. We can see that κ is very weak in the weak doping domain ($N < 10^{15}$cm^{-3}), as significant thermal transport by electrons can be observed only at high doping levels.

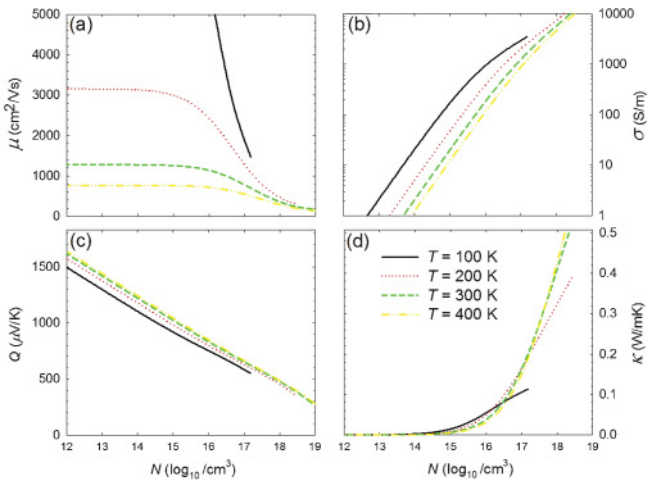

FIG. 4. (Color online) Thermoelectric properties of n-doped Si *versus* carrier concentration N at four different values of the temperature. (a) electronic mobility; (b) electrical conductivity (on a logarithmic scale); (c)Seebeck coefficient or thermal power; (d) electronic contribution to the thermal conductivity.

V. CONCLUSION

In conclusion, we have combined the Boltzmann transport equation with from-first-principles calculations of the electronic band structure and of the electron-phonon coupling constants for the intervalley scattering in silicon. This approach is developed to improve the calculation accuracy beyond the relaxation-time approximation for the determination of thermoelectric coefficients of semiconductors. The computed electronic mobility and the Seebeck coefficient at room temperature have been compared with experimental data. Good quantitative agreement has been obtained. Furthermore, temperature and doping effects on thermoelectric coefficients have been investigated in a systematic way and provide predictive data.

ACKNOWLEDGMENTS

Results have been obtained with the (modified) Quantum Espresso package.[35,46] We thank Paola Gava for the careful reading of the manuscript and many suggestions for its improvement. Useful discussions with M. Calandra, M. Lazzeri and F. Mauri are acknowledged. NM acknowledges support from Foundation Nanosciences. The authors acknowledge support from the ANR (project PNANO ACCATTONE) and computer time granted by GENCI (project 2210).

*wzzhao@yahoo.fr

[1] A. Boukai, Y. Bunimovich, J. Tahir-Kheli, J.-K. Yu, W. Goddard III, and J. Heath, Nature (London) **451**, 168 (2008).
[2] T. Harman, P. Taylor, M. Walsh, and B. LaForge, Science **297**, 2229 (2002).
[3] A. Hochbaum, R. Chen, R. Delgado, W. Liang, E. Garnett, M. Najarian, A. Majumdar, and P. Yang, Nature (London) **451**, 163 (2008).
[4] R. Venkatasubramanian, E. Siivola, T. Colpitts, and B. O'Quinn, Nature (London) **413**, 597 (2001).
[5] D. Wang, L. Tang, M. Long, and Z. Shuai, J. Chem. Phys. **131**, 224704 (2009).
[6] M. W. Oh, D. M. Wee, S. D. Park, B. S. Kim, and H. W. Lee, Phys. Rev. B **77**, 165119 (2008).
[7] B.-L. Huang and M. Kaviany, Phys. Rev. B **77**, 125209 (2008).
[8] D. J. Singh, Phys. Rev. B **76**, 085110 (2007).
[9] G. B. Wilson-Short, D. J. Singh, M. Fornari, and M. Suewattana, Phys. Rev. B **75**, 035121 (2007).
[10] H. Hazama, U. Mizutani, and R. Asahi, Phys. Rev. B **73**, 115108 (2006).
[11] G. Madsen, J. Am. Chem. Soc. **128**, 12140 (2006).
[12] G. Madsen and D. Singh, Comput. Phys. Commun. **175**, 67 (2006).
[13] F. Ishii, M. Onoue, and T. Oguchi, Physica B **351**, 316 (2004).
[14] T. Thonhauser, T. J. Scheidemantel, J. O. Sofo, J. V. Badding, and G. D. Mahan, Phys. Rev. B **68**, 085201 (2003).
[15] F. Murphy-Armando and S. Fahy, Phys. Rev. B **78**, 035202 (2008).
[16] O. Restrepo, K. Varga, and S. Pantelides, Appl. Phys. Lett. **94**, 212103 (2009).
[17] T. Dziekan, P. Zahn, V. Meded, and S. Mirbt, Phys. Rev. B **75**, 195213 (2007).
[18] D. Yu, Y. Zhang, and F. Liu, Phys. Rev. B **78**, 245204 (2008).
[19] D. Broido, M. Malorny, G. Birner, N. Mingo, and D. Stewart, Appl. Phys. Lett. **91**, 231922 (2007).
[20] A. Ward, D. A. Broido, D. A. Stewart, and G. Deinzer, Phys. Rev. B **80**, 125203 (2009).
[21] C. Jacoboni and L. Reggiani, Rev. Mod. Phys. **55**, 645 (1983).
[22] M. V. Fischetti, Phys. Rev. B **44**, 5527 (1991).
[23] D. L. Rode, Phys. Status Solidi B **53**, 245 (1972).
[24] N. W. Ashcroft and N. D. Mermin, *Solid State Physics* (Holt-Saunders, Philadelphia, 1976), pp. 244–262.
[25] D. L. Rode, in *Semiconductors and Semimetals*, (Academic, New York, 1995), p. 1.
[26] B. R. Nag, *Theory of Electrical Transport in Semiconductors* (Pergamon, Oxford, 1972), pp. 135–138.
[27] J. Sjakste, N. Vast, and V. Tyuterev, Phys. Rev. Lett. **99**, 236405 (2007).
[28] J. Sjakste, V. Tyuterev, and N. Vast, Phys. Rev. B **74**, 235216 (2006).
[29] J. Sjakste, V. Tyuterev, and N. Vast, Appl. Phys. A **86**, 301 (2007).
[30] J. Sjakste, N. Vast, and V. Tyuterev, J. Lumin. **128**, 1004 (2008).
[31] V. Tyuterev, J. Sjakste, and N. Vast, Phys. Rev. B **81**, 245212 (2010).
[32] P. Hohenberg and W. Kohn, Phys. Rev. **136**, B864 (1964).
[33] W. Kohn and L. Sham, Phys. Rev. **140**, A1133 (1965).
[34] S. Baroni, P. Giannozzi, and A. Testa, Phys. Rev. Lett. **58**, 1861 (1987).
[35] S. Baroni, S. de Gironcoli, A. Dal Corso, and P. Giannozzi, Rev. Mod. Phys. **73**, 515 (2001).
[36] P. Giannozzi, S. de Gironcoli, P. Pavone, and S. Baroni, Phys. Rev. B **43**, 7231 (1991).
[37] *Landolt-Börnstein, Semiconductors: Physics of Group IV Elements and III-V Compounds*, edited by O. Madelung, H. Weiss, and M. Schulz (Springer-Verlag, Berlin, 1982). Vol, 17a.
[38] R. Brent, *Algorithms for Minimization Without Derivatives* (Prentice-Hall, 1972).
[39] G. Gilat and L. J. Raubenheimer, Phys. Rev. **144**, 390 (1965).
[40] W. J. Patrick, Solid-State Electron **9**, 203 (1966).
[41] F. J. Morin and J. P. Maita, Phys. Rev **96**, 28 (1954).
[42] I. Granacher, J. Phys. Chem. Solids **24**, 231 (1967).
[43] T. H. Geballe and G. W. Hull, Phys. Rev. **98**, 940 (1955).
[44] J. M. Ziman, *Electrons and Phonons: The Theory of Transport Phenomena in Solids* (Oxford University Press, Oxford, 1960), pp. 421–444.
[45] Z. Wang and N. Mingo, Appl. Phys. Lett. **97**, 101903 (2010).
[46] P. Giannozzi, S. Baroni, N. Bonini, M. Calandra, R. Car, C. Cavazzoni, D. Ceresoli, G. Chiarotti, M. Cococcioni, I. Dabo, A. Dal Corso, S. De Gironcoli, S. Fabris, G. Fratesi, R. Gebauer, U. Gerstmann, C. Gougoussis, A. Kokalj, M. Lazzeri, L. Martin-Samos, N. Marzari, F. Mauri, R. Mazzarello, S. Paolini, A. Pasquarello, L. Paulatto, C. Sbraccia, S. Scandolo, G. Sclauzero, A. Seitsonen, A. Smogunov, P. Umari, and R. Wentzcovitch, J. Phys. Condens. Matter **21**, 395502 (2009).